

AC electroosmotic pump with bubble-free palladium electrodes and rectifying polymer membrane valves

Anders Brask, Detlef Snakenborg, Jörg P. Kutter and Henrik Bruus

Received 13th July 2005, Accepted 24th November 2005

First published as an Advance Article on the web 21st December 2005

DOI: 10.1039/b509997h

We present the design, test and theoretical analysis of a novel micropump. The purpose is to make a pump with large flow rate ($\approx 10 \mu\text{L min}^{-1}$) and high pressure capacity ($\approx 1 \text{ bar}$) powered by a low voltage $\Delta V < 30 \text{ V}$. The pump is operated in AC mode with an electroosmotic actuator in connection with a full wave rectifying valve system. Individual valves are based on a flexible membrane with a slit. Bubble-free palladium electrodes are implemented in order to increase the range of applications and reduce maintenance.

1. Introduction

Electroosmotic (EO) actuators are suitable for microfluidic applications because they can produce high pressures and precise flow. The increased interest in studying and applying them is reflected in the recent review papers (and the references therein) by Stone *et al.*,¹ Laser and Santiago,² and Squires and Quake.³

In EO actuators an electrolyte is pumped by applying an electric field to the Debye layer. This layer is formed by the ions in the electrolyte due to electric screening of the immobile charges on the walls of the liquid channels within the pump.^{4,5} High pressures ($\sim 1 \text{ kPa V}^{-1}$) and large flow rates ($\sim 1 \mu\text{L min}^{-1} \text{ V}^{-1} \text{ cm}^{-2}$) are achieved in these actuators by using capillaries or micro/nanoporous frits to form the pumping liquid channels.^{6–10}

An EO pump can be improved in several ways: the cascade-pump design lowers the driving voltage,¹¹ the addition of zwitterionic additives enhances the pressure,¹² and, as shown in our own recent work, carefully integrated ion exchange membranes increase the stability.¹³ Nevertheless, an EO pump operated continuously in DC mode, as those mentioned above, suffers from inherent problems. Electrolysis generates gas bubbles, which must be removed or recombined from the system.^{10,14} Redox reactions at the electrodes will eventually change the pH, which is a problem because the EO flow depends on it. In the case of pump stall conditions $Q = 0$ the EO flow is recirculating within the pumping channels and thereby generating pressure. The pH change introduced at the electrodes will stop the EO flow after a while when the buffer is depleted.

To overcome these problems with the DC drive, various electrokinetic devices that run in AC mode have been tested: electrothermally induced fluid flow,¹⁵ surface-electrode driven EO flow,¹⁶ and travelling wave EO flow.¹⁷ Common to these devices is that although the flow rates (measured in $\mu\text{L min}^{-1} \text{ V}^{-1} \text{ cm}^{-2}$) are comparable to the above mentioned, their pressure capacities are low, typically only $1\text{--}10 \text{ Pa V}^{-1}$.

The main application of these devices is manipulation of suspended particles.

In this paper we combine the high pressures and large flow rates (measured in $\mu\text{L min}^{-1} \text{ V}^{-1}$) of the porous or frit-based DC EO pump with the advantage of bubble-free AC operation. This is achieved by mounting a novel rectifying valve system based on polymer membranes onto our recently developed DC EO pump.¹³ As a second novelty, we suppress the generation of bubbles by employing palladium electrodes that can store and release hydrogen reversibly.

The paper is organized in the following way: in Sec. 2, we introduce the general concept of the pump and its novel features. The EO actuator used in this context has been described in a previous paper,¹³ hence only a brief description of it is given in Sec. 3. The palladium electrodes are described in detail in Sec. 4, while the rectifying valve system is described in Sec. 5. Integration issues such as compliance are discussed in Sec. 6. The pumping results are presented in Sec. 7 and, finally, we give an outlook and draw conclusions in Secs. 8 and 9, respectively.

2. General concept

Operating a symmetric EO pump in AC mode does not give any net flow if no net current is drawn. The flow will only oscillate back and forth. Hence, we introduce a system of rectifying valves, see Fig. 1. When the valve system is coupled to the oscillating EO actuator a net rectified flow is generated. This system is very similar to existing piezo-actuated membrane pumps.² The main difference is the actuator type and the number of valves. Also note that depending on the stroke volume the pumped liquid may enter and exit the valve system without ever entering the EO actuator. In this way the AC EO pump is less dependent on the pumped liquid than conventional DC EO pumps and with a separator system it could be completely independent.

Another difference between a conventional membrane pump and this pump is that the force from the actuator is directly applied to the liquid without the use of a displacement chamber. The disadvantage of this is that the actuator liquid may get mixed with the pumped liquid. The main advantages,

MIC—Department of Micro and Nanotechnology Technical University of Denmark, DTU bldg. 345 east, DK-2800, Kongens Lyngby, Denmark

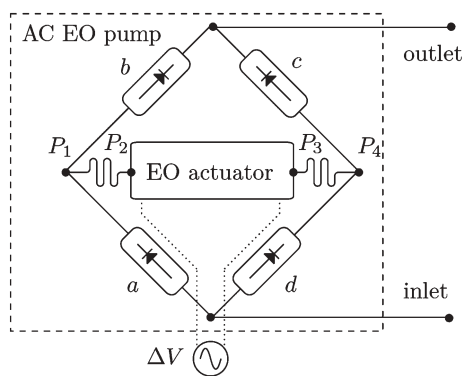


Fig. 1 Diagram of the AC EO pump with four rectifying valves *a*, *b*, *c*, and *d*. The components and channels within the dashed box constitute the AC EO pump. The solid lines are fluid channels while the dotted lines are electrical wires. The four-way valve system ensures that both stroke directions generate flow in contrast to a two-way valve system where only one stroke direction generates flow. If the driving voltage is positive, the flow goes from the inlet through valve *a*, the EO actuator and valve *c* to the outlet. For negative voltage, the flow goes from the inlet through valve *d*, the EO actuator and valve *b* to the outlet. The black dots marked P_1 – P_4 are used to explain Fig. 4.

on the other hand, are a simple design and less compliance from, *e.g.*, trapped bubbles.

3. EO actuator

The EO actuator design is based on the DC EO pump presented by Brask *et al.*¹³ The original frit-based EO pump features ion exchange membranes to separate the electrode reservoirs from the pumping loop. The present pump configuration is almost the same as described earlier and differs only in two areas. (1) The ion exchange membrane support has been improved in order to accommodate the low compliance requirements. (2) Platinum (Pt) electrodes have been replaced by bubble free palladium (Pd) electrodes allowing for a more encapsulated reservoir with less maintenance.

The essential parameters for an AC actuator are the stroke volume V_s and the pressure capacity Δp at a given current I and period T . Using the $Q/I - \Delta p/I$ data in ref. 13 we find that the maximum flow rate and pressure capacity are $Q/I = 6 \mu\text{L min}^{-1} \text{mA}^{-1}$ and $\Delta p/I = 7 \text{ bar mA}^{-1}$, respectively for a buffer concentration of $c = 20 \text{ mM}$.

In AC mode the current behaves in a highly nonlinear manner because of the depletion of the buffer close to the ion exchange membranes. For more information see ref. 13. We therefore base the performance estimates on an average value over a stroke period. At $\Delta V = 30 \text{ V}$ and $c = 20 \text{ mM}$ the current will be in the range $I = 1\text{--}5 \text{ mA}$, see Fig. 13 in Sec. 7.3, where $I = 1 \text{ mA}$ is the stationary current and $I = 5 \text{ mA}$ is immediately after the voltage switch. With a half period of $T/2 = 30 \text{ s}$ the average current will be approximately $I = 2 \text{ mA}$. This should give a stroke volume of $V_s = 6 \mu\text{L}$. With respect to the pressure capacity it is the current at the end of the stroke that matters. The pressure capacity of the actuator should be approximately $\Delta p = 10 \text{ bar}$.

4. Bubble-free electrodes

When drawing a current from an inert electrode material, *e.g.*, platinum, in an aqueous solution electrolysis happens. Oxygen is formed at the anode and hydrogen at the cathode. These gases pose a problem for long-term operation since they need to be removed.

Some metals, in particular palladium (Pd), have a high permeability for hydrogen. Running the pump in AC mode will make each electrode work as an anode and a cathode for an equal amount of time. If the hydrogen generated during the cathodic half-cycle is stored in the palladium and removed during the anodic half-cycle, the electrodes will be bubble-free.

The aim of this section is to analyze the bubble formation mechanism and hereby predict the conditions for bubble-free operation.

4.1. The bubble formation model

Hydrogen is introduced to the Pd phase through cathodic processes in aqueous media. A maximum H/Pd ratio of 0.57 is reported in ref. 18. Using the values for density $\rho_{\text{Pd}} = 12.02 \times 10^3 \text{ kg m}^{-3}$ and molecular weight $M_{\text{Pd}} = 0.106 \text{ kg mol}^{-1}$ we can estimate the maximum concentration of hydrogen to be stored $c_{\text{H,max}} = 0.57c_{\text{Pd}} = 6.4 \times 10^4 \text{ mol m}^{-3}$.

The governing transport mechanism of hydrogen in palladium is diffusion represented by the diffusion constant D . We assume that there exists a critical surface concentration of H, c_{full} . If this ratio is exceeded bubbles will be formed. c_{full} does not equal $c_{\text{H,max}}$ because of energy barriers associated with the phase transition from the aqueous to the palladium phase.

There are two characteristic time scales in this problem. The first one is the diffusion time scale, T_{diff} . At approximately this time hydrogen will have reached the core of the electrode. The second time scale is the time it takes for the electrode to saturate, T_{sat} .

$$T_{\text{diff}} = \frac{a^2}{D} \quad (1)$$

$$T_{\text{sat}} = \pi a^2 L_{\text{Pd}} c_{\text{H}} F I^{-1} \quad (2)$$

$$T_{\text{diff}}/T_{\text{sat}} = I(\pi L_{\text{Pd}} D c_{\text{H}} F)^{-1} \quad (3)$$

where a and L_{Pd} are the radius and the length of the electrode, respectively. If the ratio between diffusion time T_{diff} and filling time T_{sat} is higher than unity the surface will saturate much faster than the core. This regime is referred to as surface filling. In the case of a small ratio the concentration distribution is more uniform and both core and surface will saturate roughly at the same time. This regime is referred to as core filling.

4.2. Experiments

The bubble-free electrodes were tested in an open reservoir filled with 5 mM phosphate buffer at pH = 6.5. Two spiral shaped palladium wires of length $L_{\text{Pd}} = 40 \text{ mm}$ and diameter $2a = 0.25 \text{ mm}$ were attached to mobile plates in a long slender reservoir, 2 cm wide, 3 cm deep, and 20 cm long. The hydrogen was removed from the Pd wire by running the wire as an anode. When it was empty (bubbles of O_2 started to form) the current would be reversed and the clock started. After the time T_{bub}

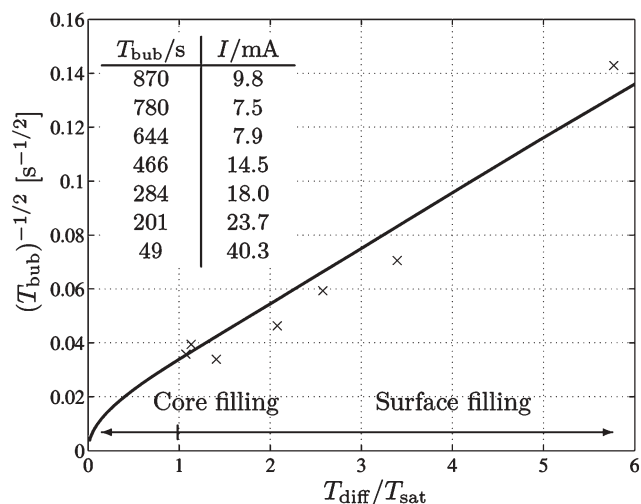


Fig. 2 Experiments (×) and simulation (solid line) of the bubble formation time $T_{\text{bub}}^{-1/2}$ vs. the ratio between diffusion time and filling time. The linear regime is denoted surface filling because the hydrogen does not reach the core before bubbles emerge ($c(r = a) > c_{\text{full}}$). In the core filling regime the diffusion is fast compared to the filling and the hydrogen is everywhere. Parameters: $D = 1.0 \times 10^{-11} \text{ m}^2 \text{ s}^{-1}$, $L_{\text{Pd}} = 40 \text{ mm}$, $c_{\text{full}} = 4 \times 10^4 \text{ mol m}^{-3}$.

bubbles of H_2 would start to form and the clock was stopped. The current was varied by changing the distance between the electrodes in the range of 2–20 cm. A Pd electrode completely loaded with hydrogen would emit bubbles even after the current was stopped. The surface of the Pd would also darken and become rougher after some cycles. However, this did not seem to affect the performance over a time scale of a couple of weeks.

4.3. Results

The experimental and model data are plotted in Fig. 2. The parameters c_{full} and D in the numerical diffusion model are chosen in order to give the best fit with the experimental data.

Consider a Pd electrode from which a constant current I is drawn. First we need to determine the ratio between diffusion and filling time, eqn (3).

$$T_{\text{bub}} = 5.7 \times 10^7 \frac{\text{A}^2 \text{s}}{\text{m}^4} i^{-2} \text{ for } T_{\text{diff}}/T_{\text{fill}} > 1 \quad (4)$$

$$T_{\text{bub}} = \frac{c_{\text{full}}}{c_{\text{H}}} T_{\text{fill}} \text{ for } T_{\text{diff}}/T_{\text{fill}} < 1 \quad (5)$$

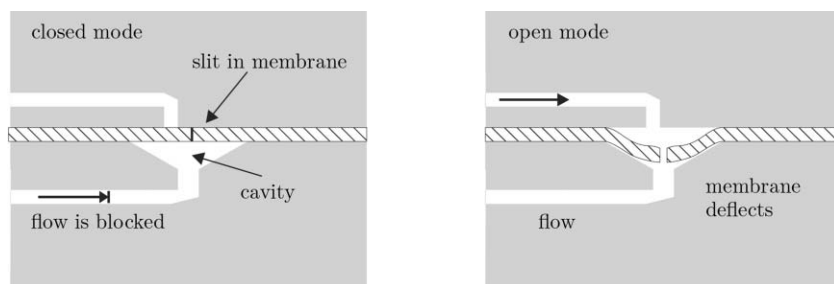


Fig. 3 This passive membrane valve is pre-loaded because no material was removed when the slit was cut. Hence the slit is so narrow that fluid will not pass without a substantial pressure drop that will compress the slit even further. Note that the inlet is slightly offset to the slit in order to make the valve more tight.

where $i = I/A$ is the current density. In the case of $I = 2 \text{ mA}$, $L_{\text{Pd}} = 40 \text{ mm}$, $a = 0.125 \text{ mm}$, and $D = 1 \times 10^{-11} \text{ m}^2 \text{ s}^{-1}$ we get the ratio $T_{\text{diff}}/T_{\text{fill}} = 0.26$. This means that we are in the core filling regime, see Fig. 2, $T_{\text{bub}} = 3.8 \times 10^3 \text{ s}$ or roughly 1 h. The stroke period of the pump is kept at a much smaller value than T_{bub} to ensure bubble-free operation.

5. Valve system

The purpose of the valve system is to rectify the pulsating flow. In order to do that the individual valves must fulfill some requirements. The actuator can supply flow rates in the order $1\text{--}10 \mu\text{L min}^{-1}$ and pressures in the range $1\text{--}10 \text{ bar}$. The valves should open at a low pressure $\approx 0.1 \text{ bar}$ and be as tight as possible. The valve module is separated from the actuator module in order to increase the flexibility. In the following we present a simple but effective valve design based on a planar membrane with a slit. The chosen approach allows fast and easy fabrication using polymer materials.

5.1. Valve design

Membrane valves are suitable for microfluidic systems because the planar design is easy to integrate. Today membrane valves are commonly used in microfluidics as pressure actuated active valves.^{19,20} The presented valve is a passive membrane valve design inspired by commercially available miniature valves such as duckbill and umbrella valves.²¹

The valve consists of a flexible membrane in which a slit or cross has been made. The membrane is placed between a rigid plane with an inlet hole on one side and a cavity with an outlet hole on the other side, see Fig. 3. The valve opens when the membrane is deflected into the cavity and hereby expands the slit or cross. The slit or cross is made with a sharp tool so that no material is removed. This is an important point because it means that the valve is pre-loaded, *i.e.*, it takes a certain pressure to open the valve.

In microfluidics the lack of inertial forces requires that microvalves are pre-loaded, in order to prevent leakage. The amount of pre-loading is governed by the thickness and Young's modulus of the membrane and by the cavity diameter.

The hypothesis is that the valve will open when the ratio between membrane deflection and thickness reaches a certain threshold. It is, however, not easy to measure the deflection precisely. Instead, we measure the pressure drop across the membrane and calculate the deflection. In ref. 22 an analytical

expression for the small deflection of a thin circular membrane with clamped edges is given as

$$u = \frac{3pa^4}{16t^3E}(1-\nu^2), \quad (6)$$

where u is the center deflection, p is the pressure drop across the disc, a is the radius of the disc, ν is Poisson's ratio, E is Young's modulus, and t is the thickness of the disc. The analytical expression is only accurate if $u < t$ and $t \ll d$. For the given membrane geometries numerical simulations indicate that the error is less than 20%, Table 1.

5.2. Material properties

The governing material parameters for the membrane deflection are the thickness t , Poisson's ratio and Young's modulus E . Young's modulus was indirectly measured by the gravitational deflection of a beam clamped at only one end.

$$E = \frac{3}{2}\rho g \frac{l^4}{ut^2} \text{ for } t \ll l \text{ and } u < t, \quad (7)$$

where $\rho = m_{\text{beam}}/(Ltb)$ is the density, g the gravitational acceleration, u the deflection, l the length of the freely suspended part of the beam, and t the thickness of the beam. A stage could be adjusted in the vertical direction with micrometer precision. The stage would start in a low position and then be gradually raised until it made contact with the tip of the beam. In some cases the beam would be attracted to the stage by static electricity. In those cases the deflection would be recorded when the tip of the beam was aligned with the edge of a spacer of known thickness. Membrane samples were cut by laser into beams of length $L = 30$ mm, width $b = 6$ mm and mass m_{beam} . The thickness t was measured by a micrometer screw gauge.

Silicone and latex have been used as membrane materials from Medical silicones (Denmark) and Ansell Medical (Germany). The membrane material has to be compatible with the bonding temperature. It was our experience that the latex membranes sometimes would get sticky after bonding, which could increase the initial opening pressure. The silicone membranes did not show any signs of change. Several different silicone compounds were tested with Young's modulus ranging from $E = 1.6$ –11 MPa and thicknesses $t = 220$ –470 μm . Poisson's ratio is assumed to be $\nu = 0.48$, which is a common value for an elastic medium such as latex or silicone. In this paper, we present only two membrane types, namely latex, $t = 220$ μm , $E = 1.2$ MPa, and silicone $t = 220$ μm , $E = 3.1$ MPa.

Table 1 Calculations of the membrane deflection u . Two methods are used: 1D axi-symmetric finite element simulations in Femlab 3.1 and the analytical approximation from eqn (6). Parameters: $p/E = 10^{-3}$, $t = 220$ μm , $\nu = 0.48$. The solved equations are linear, so $u \propto p/E$ for small deflections

d/mm	3.5	2.6	2.4	2.0
$u_{\text{sim}}/\mu\text{m}$	134	44.5	35.7	16.9
$u_{\text{an}}/\mu\text{m}$	127	38.7	28.1	13.6
Deviation (%)	4.9	13	15	20

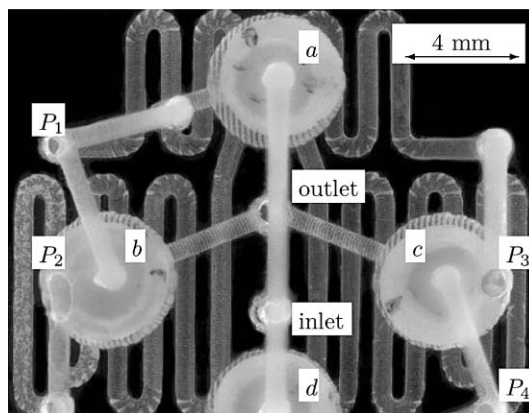


Fig. 4 Picture of the valve system from above. The three-dimensional system allows channels to cross in different levels. In the top level we have the access points P_2 and P_3 that connect to the EO actuator, see Fig. 1. In the bottom level we have the inlet and outlet of the pump. a – d are the four circular rectifying membrane valves. When the flow enters a valve from above, it can pass through the slit in the membrane (not visible). Valve b and c are connected to the outlet and a and d to the inlet. In the bottom layer two meandering channels can be seen. They connect P_1 with P_2 and P_3 with P_4 , respectively. The functionality of this layer is described in Sec. 8.

5.3. Valve fabrication

A valve system consists of five 1 mm thick polymethylmethacrylate layers. Channels are made by laser ablation^{23,24} with a 65 W CO₂ laser. After laser machining and assembly the layers are aligned using pinholes and bonded in an oven at 108 °C for 90 min.

The middle layer accommodates four circular membranes, see Fig. 4. The membranes are sealed by a circular protruding rim (not visible) along the perimeter so that no liquid can bypass the membrane radially.

Using a custom-made cut tool slits in the membranes are made in the center of the membrane. The tool consists of a stainless steel knife blade, a holder and a cut template, see Fig. 5. The length of the slit is determined by the length of the blade. The blade comes from a Stanley hobby knife and measures 8 mm in length and 0.5 mm in width (away from the edge). The blade was then thinned down to a length of 1.8 mm

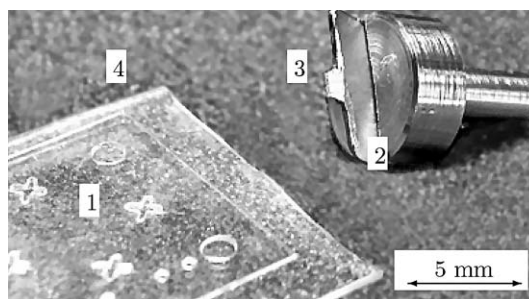


Fig. 5 Tools for making precision cuts. (1) Template made in polymer by laser ablation. (2) Knife holder that fits into a drill press. (3) Blade thinned down to the appropriate length. (4) A soft cut plate is placed beneath the membrane to ensure that the cut tool penetrates the membrane.

resulting in a 1.5 mm slit for a $t = 220 \mu\text{m}$ thick membrane. For optimum durability the blade was rounded at the edges to prevent the slit from expanding over time. The knife holder is fitted into a drill press to ensure a perfect vertical alignment. The tool does not remove any material and the slit is therefore extremely thin (or nonexistent) when the membrane is relaxed.

The geometry of the valve allows the slit to expand when pressure is applied in the positive direction of the valve. One the other hand, the slit is compressed when the pressure is in the negative direction of the valve.

5.4. Valve characterization

The Q - p characteristics of the valves were measured using an automated setup. During the measurements eight variables were sampled at 1 Hz into a data file using LabView with a 16-bit data acquisition card (National Instruments, Austin, TX, USA). The variables are voltage ΔV , current I , upstream pressure p_1^{sens} , downstream pressure p_2^{sens} , mass m of liquid in the reservoir, valve state, pressure state and elapsed time. The valve and pressure state are used in the postprocessing of the data.

The flow switching and pressure regulation were programmed in LabView. A digitally controlled amplifier circuit was constructed to control the flow switching valves (1–4) and the pressure regulation valves (5–6). All electroactuated valves (1–6) are from Lee Company (Westbrook, CT, USA), see Fig. 6.

The pressure is increased when valve (5) is open and decreased when valve (6) is open. The valves are never open at the same time. The rate at which the pressure increases or decreases \dot{p} depends on the external N_2 pressure, the variable flow resistance (7) and the volume of the N_2 reservoir. The valve positions are only updated once per second so the pressure rate \dot{p} should be adjusted accordingly. If \dot{p} is too large the pressure will oscillate around the target pressure and if it is too small the regulation will be slow.

Each valve system has four individual valves denoted a – d , see Fig. 1. Each valve is tested in both directions at 6 different

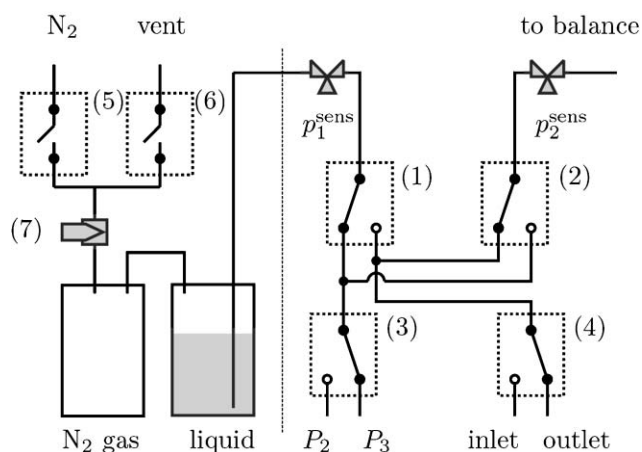


Fig. 6 The flow can be diverted into the ports P_2 , P_3 , inlet, outlet by four 3-way valves (1–4). The position depicted is c open, $P_3 \rightarrow$ outlet. The flow is driven by pressurized liquid reservoirs. The N_2 pressure is controlled by two shut valves (5–6). The regulation speed can be adjusted by a needle valve with variable flow resistance (7).

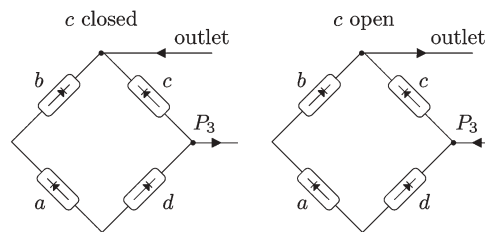


Fig. 7 Examples of the two possible valve testing configurations for valve c . In the closed case the valve is tested in parallel to a combination of b closed, a closed and d open in series. In the open case open and close are interchanged. The meander is not included in this figure.

pressures $p_1^{\text{sens}} - p_2^{\text{sens}} = (0.05, 0.1, 0.15, 0.2, 0.25, 0.3)$ bar. This equals 48 measurements of Q and p for each valve chip. The tests of the individual valves are not completely decoupled. When testing, e.g., valve c open ($P_3 \rightarrow$ outlet) we are actually measuring c open connected in parallel to a serial connection of d closed, a open and b open, see Fig. 7. At a given pressure each valve is tested for $T_{\text{meas}} = 70$ s. The first 5 s worth of data is removed because the switching of the external valves may transmit a disturbing pulse to the balance. Corresponding values of flow rate Q and pressure p are average values over the period of a measurement.

A valve is defined open when the hydraulic conductance is 10% of the maximum value at 0.3 bar. The opening pressure is found at the intersection between the 10% level and the spline for the hydraulic conductance, see Fig. 8.

A series of experiments with different sized cavities were performed. The purpose was to see the effect of cavity size d on the opening pressure p_{open} , Fig. 9. It is seen that the opening pressure increases greatly with decreasing cavity diameter.

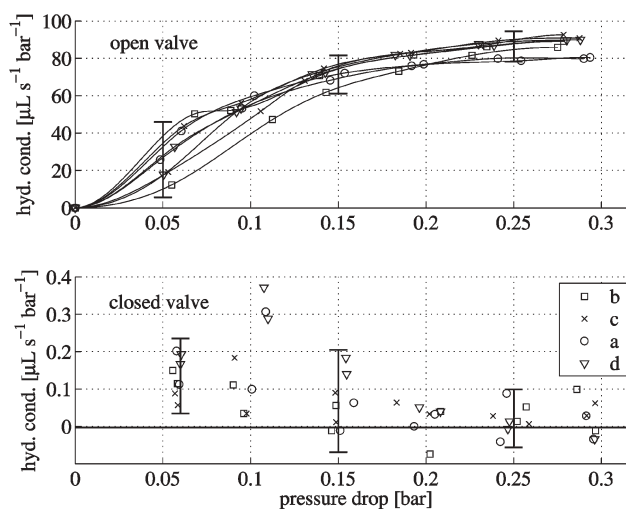


Fig. 8 Q - p characteristic for four valves with $t = 220 \mu\text{m}$ latex membrane, 2.9 mm cavity, and 1.8 mm slits, $E = 1.2$ MPa. Two identical experiments were conducted to test the reproducibility. The diodicity is in excess of 10^2 and the valves have very little resistance in the open mode. The negative flow measurements are due to noise on the balance readings. This particular valve system was used in all of the pumping experiments. The error bars indicate the $\pm 2\sigma$ level for three selected pressure drops.

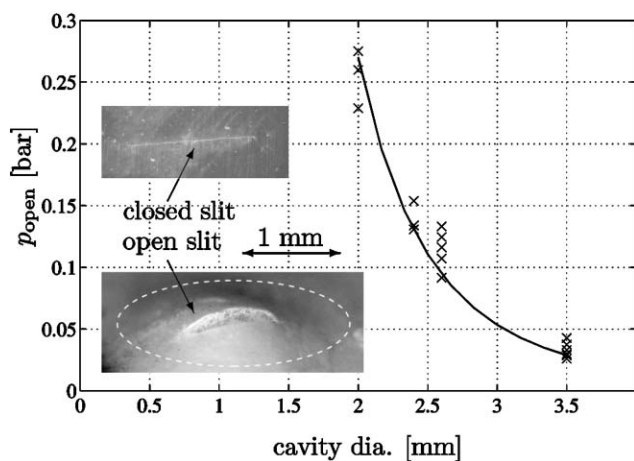


Fig. 9 Opening pressure p_{open} vs. cavity diameter d . p_{open} is defined as the pressure where the hydraulic conductance is 10% of the maximum value (at 0.3 bar). The solid line is a polynomial fit $p_{\text{open}} \propto d^{-4}$. The insets show a relaxed membrane with a closed slit and a deflected membrane with an open slit. The dashed line is the perimeter of the membrane. Parameters: silicone valve system $t = 220 \mu\text{m}$, $E = 3.1 \text{ MPa}$.

The opening pressure is seen to follow a $p_{\text{open}} \propto d^{-4}$ dependence. Combining this information with the deflection $u \propto d^4$ from eqn (6) we conclude that the membrane deflection needed for valve opening is constant. Using the opening pressures from Fig. 9 we may calculate the deflection ratio ult , see Table 2.

Additional valve tests indicated that the ratio ult is constant independent of the thickness t , cavity diameter d and Young's modulus E (using eqn (6) and $ult = \text{const.}$). Using this approximation we arrive at a simple scaling model for the opening pressure, $p_{\text{open}} \propto E (t/a)^4$. The scaling model states that smaller valves with similar opening pressures are possible as long as the ratio between the membrane thickness t and cavity radius a is kept constant. According to this scaling a miniature valve with a diameter of $2a = 1 \text{ mm}$, and membrane thickness of $t = (1 \text{ mm}/2.6 \text{ mm}) \times 220 \mu\text{m} = 85 \mu\text{m}$, and an opening pressure of $p_{\text{open}} = 0.1 \text{ bar}$ should be possible.

6. Integration issues

The integration of the different pump components is very important. The pump is constructed in modules that can be separated. In this section we describe some of the integration issues. Some of these issues are trivial while others are more advanced. The integrated pump is shown in Fig. 10.

Table 2 The deflection ratio ult vs. cavity diameter. The results indicate that for a given membrane thickness t there exists a $ult \approx 0.7$ ratio where the valve opens. The mean values are all within the standard deviations. Parameters: $t = 220 \mu\text{m}$, $E = 3.1 \text{ MPa}$, silicone, slit: 1.8 mm

Cavity diameter/mm	Mean ult	Standard deviation ult
2.0	0.61	0.07
2.4	0.66	0.07
2.6	0.72	0.09
3.5	0.63	0.11

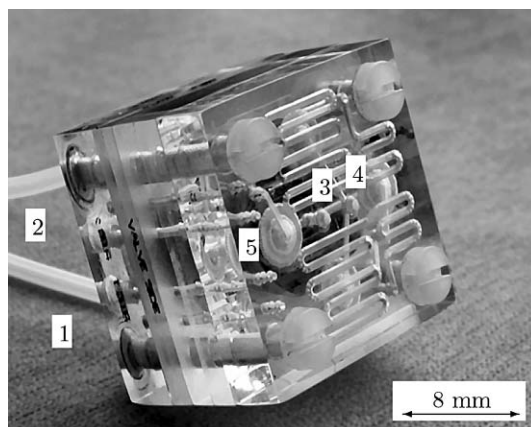


Fig. 10 Picture of the assembled pump. Tubes (1) and (2) connect to the EO actuator via P_2 and P_3 , respectively. These external connections are only used for priming of the pump and are sealed off during operation. The inlet and outlet of the pump are marked (3) and (4), respectively (no tubes are attached for better visibility). (5) The valve system is seen from the opposite side compared to Fig. 4.

6.1. Leaks

The pump is constructed in layered modules. Some of the layers are thermally bonded while others are mechanically compressed to form a seal. Cavities within the polymer layers or gaskets may give rise to a nonuniform compression with resulting leaks. This effect is nontrivial and has to be considered when designing the flow system. More trivial causes for leaks or unintended cross flow are poor bonding or loose external tubing.

6.2. Sealing

The pump is held together by four custom fabricated polycarbonate $M2 \times 20 \text{ mm}$ bolts. Initially, stainless steel bolts were used because of their good mechanical properties. However, it was found that the bolts made electrical contact with the buffer through the ion exchange membranes. Voltage differences in excess of 2 V existed between the bolts. This was unacceptable because it meant that there were stray currents, hence the need for nonconducting bolts. The polycarbonate bolts are much weaker mechanically but still strong enough to give the necessary compression.

6.3. Internal flushing system

Thermally bonded parts are thoroughly tested for functionality after bonding. This is necessary because bonded channels can be deformed if the bonding pressure or temperature was too high. Aligning of interconnections between layers is also critical. If holes are misaligned no fluid can pass.

In the actuator some of the channels are defined by the gasket layers. This type of design can give problems because of the flexible nature of the gaskets. Hence, the channel dimensions depend on the compression of the layers at assembly. Sometimes the channels would be completely blocked. To some degree this was solved by minimizing the amount of gasket defined channels.

After assembly the hydraulic resistance of the internal flushing system is evaluated. This value should be low in order not to give any considerable internal pressure drop during operation.

6.4. Compliance

The actuator and the valve system specifications have to match in order for the pump to function properly. A very important integration issue is the compliance K which is defined as the derivative of the volume with respect to the pressure p .

In the DC case the compliance affects the response time of the pump but in the AC case it affects the Q - p characteristics. The main contribution to the compliance comes from the freely suspended ion exchange membranes. The frit support was changed from a relatively coarse polymer mesh (1 mm) to a fine frit (10–16 μm). By grinding the surface of the frit support a completely smooth support was obtained. However, the membrane itself has a clearance of 90 μm to each side because of the gaskets. In the worst case scenario this would yield a variable volume of $5 \times 5 \times 0.18 \text{ mm}^3 = 4.5 \mu\text{L}$. Inserting a 180 μm thick glass fibre plate reduces the clearance of the ion exchange membrane to a minimum. A typical value for the compliance is $K = 2 \mu\text{L bar}^{-1}$ for each frit compartment.

In the valve chip the flexible membranes can increase the compliance as well. Especially the cavity design is important. If the cavity is shaped as a cylinder it is very likely that air bubbles will be trapped along the perimeter of the cavity. A conical shaped cavity reduces the risk of this happening. Optimally, the cavity is shaped to match the deflection leaving almost no dead volume when the valve is fully open.

6.5. Electrical contact

The electrical resistance of the pump should be reproducible for a given buffer concentration. In order to achieve this the pump must be constructed such that it is possible to fill the electrode reservoirs and internal chambers the same way each time. Trapped air may change the electrical resistance. Using a glass frit as membrane support has a second advantage. Because of the hydrophilic nature of the porous glass a good electrical contact is easily made between the electrode chamber and the ion exchange membrane.

7. Pump characteristics

The applied voltage was controlled from LabView through a data acquisition card. The output voltage from the data acquisition card was in the range $\pm 10 \text{ V}$. By connecting this output to a 3-fold amplifier the desired voltage range could be obtained. In all experiments a square wave $V = \pm 30 \text{ V}$ was applied. The setup shown in Fig. 6 was modified to accommodate the pump between the two pressure sensors, p_1^{sens} and p_2^{sens} instead of the switching valves (1–4).

7.1. Flow rate and pressure characteristics

The first test is to measure the free flow rate, *i.e.*, no backpressure applied. In this case the flow rate should be stable over time. The pump is operated for 2 h without any noticeable

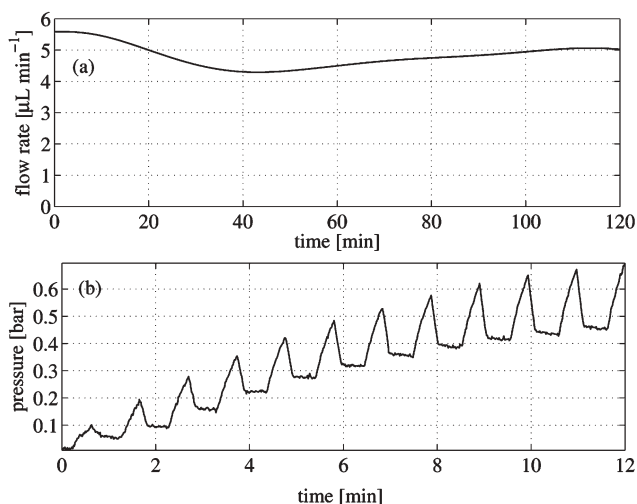


Fig. 11 (a) Average free flow rate Q vs. time. The flow rate is found as the derivative of a spline fitted to the volume vs. time data. The peaks from individual strokes are averaged out by the spline. Parameters: period $T = 40 \text{ s}$, buffer 20 mM borax, voltage $\pm 30 \text{ V}$, latex valve system, $t = 220 \mu\text{m}$, $E = 1.2 \text{ MPa}$, $d = 2.6 \text{ mm}$. (b) Backpressure p vs. time, when the outlet of the pump is blocked. The plot shows the gradual pressure buildup. There is a small amount of compliance in the pressure sensor. Parameters: same as panel (a) except the period, which is now $T = 60 \text{ s}$.

change in performance, see Fig. 11(a). The flow rate is calculated by differentiating the spline fitted to the volume vs. time data. The flow rate varies $0.5 \mu\text{L min}^{-1}$ around the mean value of $Q = 5 \mu\text{L min}^{-1}$. The actuator should supply a flow rate of $Q = 12 \mu\text{L min}^{-1}$. The reason for this discrepancy is the compliance and the efficiency of the valve system.

The pressure capacity of the pump is measured by blocking the outlet, see Fig. 11(b). The pressure builds up gradually. Apparently, only one of the stroke directions contributes to the pressure buildup. This is seen by the plateau in between the peaks. The reason could be that the compliance is different on different sides of the frit. The immediate relaxation in pressure right after the peak is probably because the valve membrane returns to its closed position. The backflow resulting from membrane movement is roughly $V_{\text{back}} = 0.5 \mu\text{L}$. The terminal pressure is approximately $\Delta p = 0.5 \text{ bar}$, which is quite low compared to the expected actuator pressure of $\Delta p = 10 \text{ bar}$. The largest pressure measured with a valve system was $\Delta p = 2 \text{ bar}$.

7.2. Flow rate dependence on stroke period

The flow rate depends on the stroke period. Two mechanisms are important. Due to ion depletion near the ion exchange membranes the current and hence the flow rate drops over time. The average flow rate of the actuator is therefore larger for a short stroke period than for a long stroke period.

If the pump is operated with a small stroke volume it is more susceptible to flow reduction because of compliance than if operated with a large stroke volume. On the other hand a pump operated with a very long period may have unnecessary low flow rate because of ion depletion. The optimum period

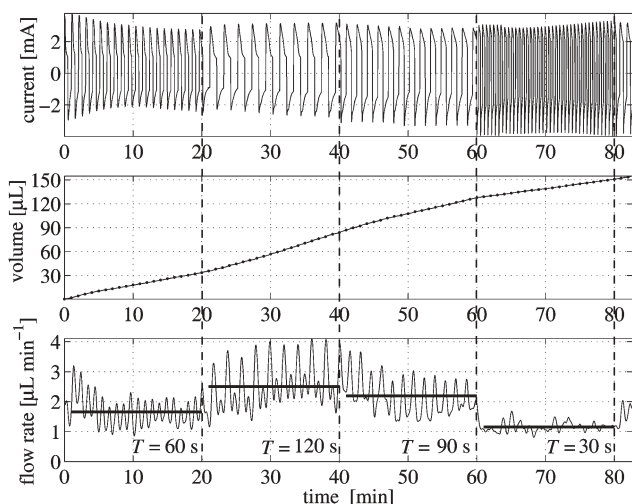


Fig. 12 Current I , volume V , and flow rate Q vs. time. The period T is varied over time: 0–20 min $T = 60$ s, 20–40 min $T = 120$ s, 40–60 min $T = 90$ s, 60–80 min $T = 30$ s. The horizontal solid lines indicate the average flow rate for each period. The flow rate Q is seen to increase with the length of the period T . Parameters: buffer 20 mM borax, voltage ± 30 V, latex valve system, $t = 220$ μm , $d = 2.6$ mm.

depends on the compliance and on the stroke volume. In Fig. 12 the flow rate Q is measured for different stroke periods.

From Fig. 12 it is seen that the flow rate increases with increasing stroke period. The stroke volumes were measured after the experiment by removing the valve chip and connecting each port P_2 and P_3 to a half filled measurement tube. The stroke volumes could then be measured by observing the moving interface in the respective tubes. In a tube with an inner diameter of $2a = 0.5$ mm there is $V_{\text{tube}} = 0.196$ $\mu\text{L mm}^{-1}$. The results were $V_{15\text{ s}} = 0.30$ μL , $V_{30\text{ s}} = 0.95$ μL , $V_{45\text{ s}} = 1.6$ μL , $V_{60\text{ s}} = 1.9$ μL . The compliance was measured by applying 1 bar of excess pressure to a measurement tube and observing how far the interface moved. The compliances on each side of the frit were measured to $K_1 = 1.5$ $\mu\text{L bar}^{-1}$ and $K_2 = 1.8$ $\mu\text{L bar}^{-1}$, respectively. The low ratio between the stroke volume and compliance implies that the pump will not

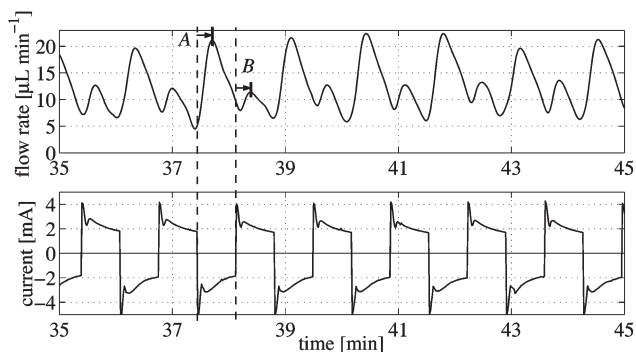


Fig. 13 Flow rate Q and current I vs. time. At position A the flow has switched from positive to negative. It takes approximately 10 s for the flow rate to respond. Then the flow rate decreases again because of the decrease in current. At position B the same thing happens with smaller amplitude. Parameters: period $T = 80$ s, buffer 20 mM borax, voltage ± 30 V, latex valve system, $t = 220$ μm , $d = 2.6$ mm.

be able to produce any significant pressure compared to the pressure capacity of the actuator.

7.3. Flow rate and current

In the actuator the flow rate and current are almost in phase. However, when coupled to nonlinear components such as the valve system a phase lag between the flow rate of the AC EO pump and the current is introduced, see Fig. 13.

The difference in flow rate in the two stroke directions indicates that there is an asymmetry in either the actuator or the valve system. We also note that the peak currents are slightly different when positive and negative voltages are applied. Such asymmetries in flow and current have been observed in almost all of the experiments.

In this case, the average flow rate is close to the predicted value of $Q = 12$ $\mu\text{L min}^{-1}$, which means that the valve system and actuator are performing well in spite of the asymmetry.

8. Outlook

Future work involves the development of a system capable of separating the buffer in the actuator from the externally pumped liquid, *e.g.*, by using oil plugs. Such a system would render the pump independent of the external liquid and hereby improve on the design idea in ref. 25 where EO induced viscous drag in a two liquid system was used as the pumping mechanism. The present design already has a separator system consisting of two meanders with side channels enabling precise positioning of separator plugs, see Figs. 4 and 10. The separator plug should stay in the meander during operation. This implies that the problems with flow drift (asymmetry in stroke volumes) and compliance must be resolved before such a system could work satisfactorily.

9. Conclusion

We have presented a novel AC electroosmotic pump with rectifying membrane valves. The pump is almost maintenance-free because of the bubble-free palladium electrodes.

The conditions for bubble-free operation of palladium electrodes have been analyzed numerically and experimentally. A simple diffusion model was found to give an adequate description of the bubble formation mechanism.

A full-wave rectifying valve system has been designed and tested successfully. The parameters governing the valve characteristics have been investigated and design guidelines have been proposed to aid in further miniaturization of the promising membrane valve concept.

The AC EO pump is more versatile than the previous DC EO pump because it is also capable of pumping buffered solutions with particles as these only have to pass the valves and not through the nanoporous frit. Because of the possibility to pump all types of liquids in a precise and controlled manner, the described concept and design bears great promise.

Acknowledgements

We would like to acknowledge Torben Jacobsen for helpful discussions on electrochemistry. This work is partly supported

by the Danish Technical Research Council, μ TAS Frame Program Grant No. 26-00-0220.

References

- 1 H. A. Stone, A. D. Stroock and A. Ajdari, *Annu. Rev. Fluid Mech.*, 2004, **36**, 381.
- 2 D. J. Laser and J. G. Santiago, *J. Micromech. Microeng.*, 2004, **14**, R35.
- 3 T. M. Squires and S. R. Quake, *Rev. Mod. Phys.*, 2005, **77**, 977.
- 4 R. J. Hunter, *Zeta Potential in Colloidal Science: Principles and Applications*, Academic Press, London, 1981.
- 5 R. F. Probstein, *Physicochemical Hydrodynamics*, Wiley, New York, 1994.
- 6 W. E. Gan, L. Yang, Y.-Z. He, R.-H. Zeng, M. L. Cervera and M. de la Guardia, *Talanta*, 2000, **51**, 667.
- 7 S. Zeng, C.-H. Chen, J. C. Mikkelsen and J. G. Santiago, *Sens. Actuators, B*, 2001, **79**, 107.
- 8 S. Zeng, C.-H. Chen, J. G. Santiago, J.-R. Chen, R. N. Zare, J. A. Tripp, F. Svec and J. M. J. Frechet, *Sens. Actuators, B*, 2002, **82**, 209.
- 9 B. P. Mosier, R. W. Crocker, J. L. Rognlien and K. D. Patel, *Am. Soc. Mech. Eng., FED*, 2003, **259**, 511.
- 10 S. Yao, D. E. Hertzog, S. Zeng, J. C. Mikkelsen and J. G. Santiago, *J. Colloid Interface Sci.*, 2003, **268**, 143.
- 11 Y. Takamura, H. Onoda, H. Inokuchi, S. Adachi, A. Oki and Y. Horiike, *Electrophoresis*, 2003, **24**, 185.
- 12 D. S. Reichmuth, G. S. Chirica and B. J. Kirby, *Sens. Actuators, B*, 2003, **92**, 37.
- 13 A. Brask, J. P. Kutter and H. Bruus, *Lab Chip*, 2005, **5**, 730.
- 14 S. Yao and J. G. Santiago, *J. Colloid Interface Sci.*, 2003, **268**, 133.
- 15 N. G. Green, A. Ramos, A. González, A. Castellanos and H. Morgan, *J. Electrostat.*, 2001, **53**, 71.
- 16 V. Studer, A. Pépin, Y. Chen and A. Ajdari, *Analyst*, 2004, **129**, 944.
- 17 A. Ramos, H. Morgan, N. G. Green, A. González and A. Castellanos, *J. Appl. Phys.*, 2005, **97**084906-1.
- 18 I.-Y. Wei and J. Brewer, *AMP J. Technol.*, 1996, **5**, 49.
- 19 C. Goll, W. Bacher, B. Bustgens, D. Maas, R. Ruprecht and W. K. Schomburg, *J. Micromech. Microeng.*, 1997, **7**.
- 20 V. Studer, G. Hang, A. Pandolfi, M. Ortiz, W. F. Anderson and S. R. Quake, *J. Appl. Phys.*, 2004, **95**, 393.
- 21 Minivalve International, Jaartsveldstraat 5a 7575 BP Oldenzaal, The Netherlands, <http://www.minivalve.com>.
- 22 W. C. Young, *Roarks Formulas for Stress and Strain*, McGraw-Hill Inc., New York, 6th edn, 1989.
- 23 H. Klank, J. P. Kutter and O. Geschke, *Lab Chip*, 2002, **2**, 242.
- 24 M. F. Jensen, M. Noerholm, L. H. Christensen and O. Geschke, *Lab Chip*, 2003, **3**, 302.
- 25 A. Brask, G. Goranović, M. J. Jensen and H. Bruus, *J. Micromech. Microeng.*, 2005, **15**, 883.